Appendix

The integral forms of the momentum and energy solutions are obtained below for the case where freestream vorticity and total enthalpy gradients are included in the boundary-layer solution. From Eqs. (1) and (2), and (8),

$$\tau_0 = \int_0^\delta \{u_x^m[(\rho u)^m - \rho u] + [\rho u(u^m - u)]_x + u_y^m[(\rho v)^m - \rho v] + [\rho v(u^m - u)]_y\}\,dy \tag{A1}$$

Equation (A1) together with Eqs. (1), (10), and (7a) then gives

$$\tau_0 = (u_x)_0^i \int_0^\delta [(\rho u)^m - \rho u]\,dy - \frac{d}{dx}\omega_0^i \int_0^\delta [(\rho u)^m - \rho u]y\,dy + \frac{d}{dx}\int_0^\delta \rho u(u^m - u)dy \tag{A2}$$

Similarly, from Eqs. (1), (4), (7b), and (10),

$$q_0 = \int_0^\delta \{H_x^m[(\rho u)^m - \rho u] + [\rho u(H^m - H)]_x + H_y^m[(\rho v)^m - \rho v] + [\rho v(H^m - H)]_y\}dy = (H_x)_0^i \int_0^\delta [(\rho u)^m - \rho u]\,dy + \frac{d}{dx}(H_y)_0^i \times \int_0^\delta [(\rho u)^m - \rho u]y\,dy + \frac{d}{dx}\int_0^\delta \rho u(H^m - H)dy \tag{A3}$$

References

[1]Melnik, R. E., "Turbulent Interactions on Airfoils at Transonic Speeds—Recent Developments," *Computation of Viscous-Inviscid Interactions*, AGARD CP-291, Oct. 1980, Paper 10.

[2]Johnston, W. and Sockol, P., "Matching Procedure for Viscous-Inviscid Interactive Calculations," *AIAA Journal*, Vol. 17, June 1979, pp. 661-663.

[3]Murman, E. M. and Bussing, T.R.A., "On the Coupling of Boundary Layer and Euler Equation Solutions," *2nd Symposium on Numerical and Physical Aspects of Aerodynamic Flows, 1983*, edited by T. Cebeci, Springer-Verlag, New York, 1984, pp. 313-326.

[4]Van Dyke, M., *Perturbation Methods in Fluid Mechanics*, Academic Press, New York, 1964.

In-Bore Velocity Measurements in the Wake of a Subsonic Projectile

A.F. Bicen,* Y. Kliafas,† and J.H. Whitelaw‡
Imperial College of Science and Technology
London, England

Introduction

VELOCITY and pressure have been measured in the flow behind a projectile traveling in a tube and propelled by compressed gas. The arrangement is intended to simulate that of interior ballistics, with nonreacting flow and projectile velocities up to 21 m/s. Although the real processes are much more complex and involve a continuous interaction of two phases (solid gas or liquid gas) through a combustion process, the present simplified experiments serve to provide fundamental understanding of the flow behind in-bore projectiles and thereby support the development of phenomenological models, such as those of Refs. 1 and 2, and multidimensional solution methods such as that of Ref. 3.

A projectile was secured in position inside a tube pressurized by compressed gas to a required pressure. After the gas had become quiescent, the projectile was released. The pressure in the tube and the projectile velocity were measured, together with the local velocity of the fluid obtained with a laser velocimeter, as a function of time. The experiment was repeated at different locations until a satisfactory picture of the flow had been assembled. The initial pressure was regarded as a variable so as to determine the extent to which the flow properties varied with projectile velocity, and the experiment was conducted with two initial chambers of different length.

Experimental System

The flow arrangement and related instrumentation are shown in Fig. 1. The measurements were obtained in the cavity formed by a 76.7-mm-diam tube, a blanked end, and a 76.4-mm-diam projectile that had a flat end. The effect of initial chamber length was investigated by using two different lengths of 177.3 and 311 mm, which were achieved by altering the projectile overall length. The upper 300 mm of the tube was made of plexiglass and the remaining part of mild steel with the gap between the projectile and tube wall sealed by two silicon-rubber rings. The projectile was allowed to travel for a distance of approximately 400 mm before being retarded by a series of compression springs.

The initial gas pressure P_i ranged from 2.91 to 9.1 bars and was achieved with nitrogen taken from a pressurized cylinder.

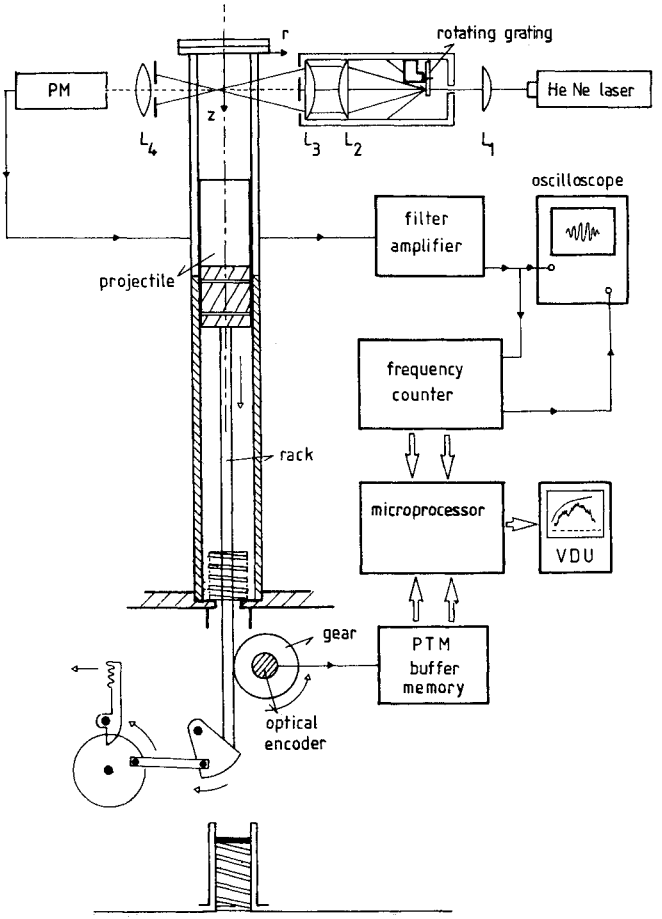

Fig. 1 Schematic diagram of experimental system.

Received April 10, 1985; presented as Paper 85-1676 at the AIAA 18th Fluid Dynamics, Plasmadynamics and Lasers Conference, Cincinnati, OH, July 16-18, 1985; revision received Aug. 26, 1985.

*Research Fellow, Department of Mechanical Engineering.

†Research Assistant, Department of Mechanical Engineering. Member AIAA.

‡Professor, Department of Mechanical Engineering.

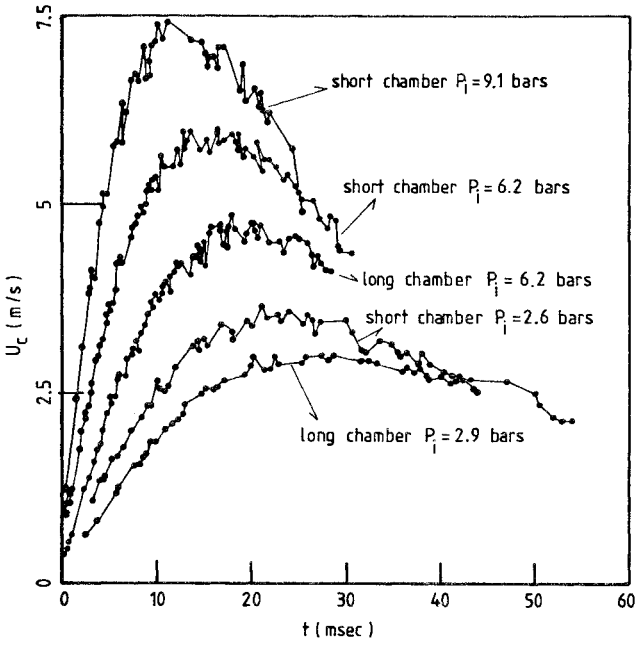

Fig. 2 Centerline velocity traces at $z=153.4$ mm for two initial chamber lengths and various initial pressures.

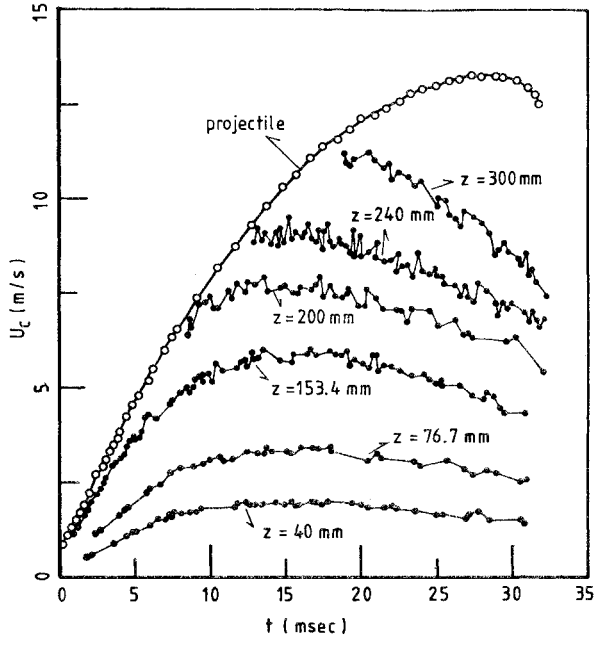

Fig. 3 Centerline velocity traces at various axial locations for short initial chamber and $P_i=6.2$ bars.

The initial pressure and the variation of pressure with time were measured, with a precision of ±.002 bar, using a piezoelectric transducer and a charge amplifier whose output was digitized and interfaced to a microprocessor.

Laser Doppler anemometry was used to obtain the fluid velocities with the optical arrangement of Ref. 4. Silicon oil droplets, served as light-scattering particles, were introduced in the initial chamber prior to the charging of the volume with the pressurized gas.

The frequency of the Doppler signal was measured by a purpose-built frequency counter also interfaced to the microprocessor. The time information corresponding to each frequency count was obtained from a Programmable Timer Module initiated to time at a rate of 417 KHz after the first 1-mm travel of the projectile.

The projectile position was determined by an optical encoder coupled to the rack and gear arrangement of Fig. 1, and each encoder pulse corresponded to an axial distance of 0.2 mm. The time between two consecutive pulses was measured by a high-frequency crystal clock oscillating at a rate of 1.0 MHz, and values were stored in a buffer memory.

The data stored were subsequently processed by the microprocessor to determine and display the variation of projectile and local flow velocity and pressure as a function of time. The accuracy of fluid velocity measurement is expected to be of the order of 1% except in the near-wall region where velocity-gradient broadening became important and, with the present optical arrangement, precluded useful results within around 0.5 mm of the wall.

Results and Discussion

The traces of centerline velocity U_c, measured at an axial distance of 153.4 mm from the closed end, are shown in Fig. 2 for both chambers and for a range of initial pressures. The velocities with the larger initial volume are lower, since the measurement location is farther from the projectile. It is also evident that each velocity trace is initially associated with a monotonic increase and that fluctuations gradually appear with decreasing acceleration. The root-mean-square value of these fluctuations is around 3%, with normalized peak-to-peak values of about 6%.

Centerline velocity traces are also shown in Fig. 3 for the short initial chamber and initial pressure of 6.2 bars. The

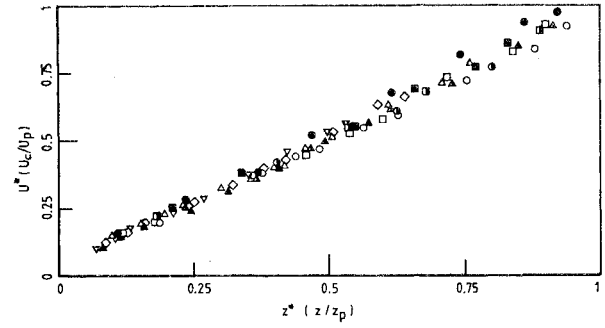

Fig. 4 Plots of nondimensional centerline velocity U^* against nondimensional axial distance z^* for long chamber and $P_i=2.91$ bars; ○ $t=5$, □ $t=10$, △ $t=20$, ◇ $t=30$, and ▽ $t=40$ ms: for long chamber and $P_i=6.2$ bars; ● $t=5$, ■ $t=10$, and ▲ $t=20$ ms: for short chamber and $P_i=6.2$ bars; ⊙ $t=5$, ⊡ $t=10$ and ⊿ $t=20$ ms.

results include some of those of Fig. 2, extend to larger values of axial distance, and include positions initially occupied by the projectile. The fluid velocity increases with axial distance and in accord with the accelerating projectile. At positions initially occupied by the projectile, the velocity decays after the projectile has passed, at a rate that increases with the axial distance. The results confirm the tendency of the fluid velocities to fluctuate with an amplitude that appears to increase until a peak-to-peak value of around 6% is achieved.

Figure 4 shows the nondimensional centerline velocity $U^*(U_c/U_p)$ plotted against the nondimensional axial distance $z^*(z/z_p)$ for different initial pressures, chamber lengths, and times in the cycle; U_p and z_p are the corresponding projectile velocity and position, respectively. The figure clearly demonstrates that the fluid velocity distribution between the breech and the projectile base is linear and scales with the projectile velocity at all times in the cycle, for the range of initial pressures and two chamber lengths considered here.

Radial profiles of velocity were obtained from velocity traces such as those of Fig. 5 and were found to be nearly uniform apart from thin regions near the wall boundaries.[4] The traces of Fig. 5 correspond to locations 0.5, 1, and 2 mm from the wall with the velocity values at $r_w=0.5$ mm generally of the order of 90-94% of the velocities at $r_w=2$ mm. The

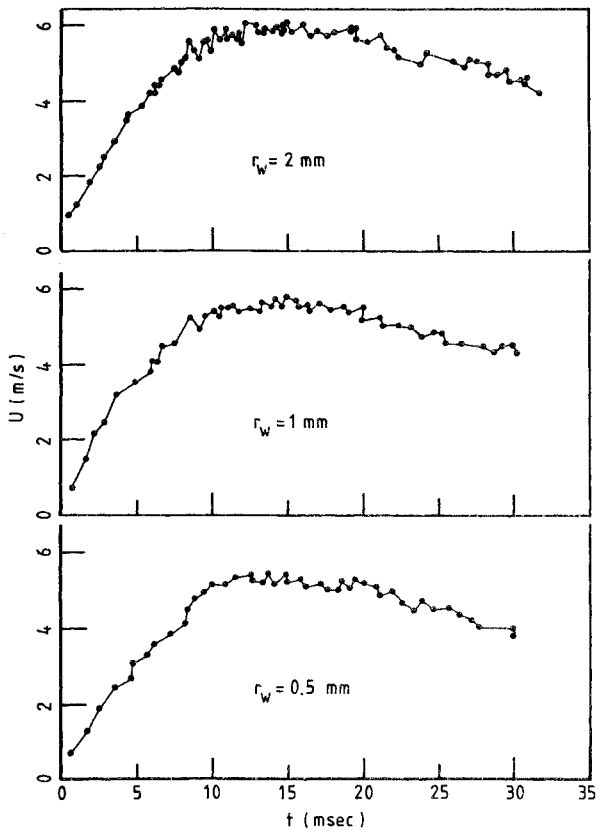

Fig. 5 Fluid velocity traces near wall boundary at $z = 153.4$ mm for short initial chamber and $P_i = 6.2$ bars.

boundary-layer thickness was found to be less than 1 mm, which corresponds to about 1% of the tube diameter. The numerical calculations of Schmitt et al.[3] predict similar boundary-layer thickness. The turbulence levels are slightly lower than those observed in the core region.

Conclusions

The main findings of this investigation are as follows:

1) The flow at any given time in the cycle is nearly one-dimensional apart from thin regions near the wall boundaries. Velocity fluctuations reach a maximum peak-to-peak value of around 6% in the core region.

2) In all cases the boundary-layer thickness is less than 1 mm, which corresponds to about 1% of the bore. The velocity fluctuations in the boundary layer are generally lower than those in the core region.

3) The velocity increases linearly with axial location from zero at the breech to that of the projectile at the base.

4) The bulk fluid velocity scales with that of the projectile, independently of initial chamber length and pressure.

Acknowledgments

The authors are pleased to acknowledge financial support provided by the U.S. Army under contract DAJA 45-84-C-0032. Useful discussions with Dr. C. Zoltani are gratefully acknowledged.

References

[1]Krier, H. and Adams, M.J., "An Introduction to Gun Interior Ballistics and a Simplified Ballistic Code," *Progress in Astronautics and Aeronautics: Interior Ballistics of Guns*, Vol. 66, edited by H. Krier and M. Summerfield, AIAA, New York, 1979, p. 1.

[2]Giovanetti, A.J. and Rife, J.M., "Internal Ballistics Model for a Liquid Monopropellant Gun," *Journal of Ballistics*, Vol. 6, No. 1, 1982, p. 1348.

[3]Schmitt, J.A., Banks, N.E., Zoltani, C.K., and Mann, T.L., "Two-Phase Viscous Flow Modeling of Interior Ballistics, Algorithm and Numerical Predictions for an Idealized Lagrange Gun," presented at the ASME Winter Annual Meeting, Washington, DC, Nov. 1981.

[4]Bicen, A.F., Kliafas, Y., and Whitelaw, J.H., "Velocity Characteristics of the Wakes of In-Cylinder Projectiles," AIAA Paper 85-1676, 1985.

Transonic Potential Flow in Hyperbolic Nozzles

Minwoo Park* and D. A. Caughey†
Cornell University, Ithaca, New York

Introduction

THE classical problem of transonic flow through a hyperbolic nozzle (see, e.g., Ref. 1) with or without a shock wave, has been revisited by applying recently developed numerical methods. Both planar and axisymmetrical cases have been considered. The full potential equation is solved in conservation form using the finite volume method of Jameson and Caughey.[2] To treat the mixed nature of the equation, either a first- or a second-order numerical viscosity in the direction of the flow is added explicitly in conservation form. A multigrid, alternating direction implicit (ADI) method[3] is used to solve the difference equations and the results are compared with analytical and numerical results of earlier researchers.

Analysis

Finite Volume Formulation

The law of conservation of mass for the isentropic flow through a nozzle can be expressed as

$$(\rho\Phi_x)_x + (\rho\Phi_y)_y = 0 \tag{1}$$

where Φ is the velocity potential and x,y Cartesian coordinates with x the axis of symmetry. Here ρ is defined as

$$\rho = \tilde{\rho} \quad \text{for planar flow}$$

$$\rho = \tilde{\rho} y \quad \text{for axisymmetric flow} \tag{2}$$

where $\tilde{\rho}$ is the fluid density which can be related to the magnitude of the velocity by the isentropic relation.

Equation (1) is transformed to a new (boundary-conforming) coordinate system (X, Y) by following the usual procedure.[2] The resulting equation can be written in terms of the contravariant velocity components (U, V) as

$$(\rho h U)_X + (\rho h V)_Y = 0 \tag{3}$$

where h is the determinant to the Jacobian matrix of the transformation.

A finite difference approximation is constructed by representing the Cartesian coordinates and the solution within each mesh cell using a bilinear mapping. Flux

Received May 9, 1985; revision received Aug. 29, 1985.

*Graduate Research Assistant, Sibley School of Mechanical and Aerospace Engineering. Student Member AIAA.

†Professor, Sibley School of Mechanical and Aerospace Engineering. Associate Fellow AIAA.